Molecular Crystals and Liquid Crystals
Publication details, including instructions for authors and subscription information:
http://www.tandfonline.com/loi/gmcl20

Nematicon Self-Steering

Armando Piccardi [a] , Alessandro Alberucci [a] & Gaetano Assanto [a]
[a] NooEL, Nonlinear Optics and OptoElectronics Lab, University "Roma Tre", Via della Vasca Navale 84, Rome-Italy

Version of record first published: 07 Oct 2011

To cite this article: Armando Piccardi, Alessandro Alberucci & Gaetano Assanto (2011): Nematicon Self-Steering, Molecular Crystals and Liquid Crystals, 549:1, 1-9

To link to this article: http://dx.doi.org/10.1080/15421406.2011.581119

Mol. Cryst. Liq. Cryst., Vol. 549: pp. 1–9, 2011

ISSN: 1542-1406 print/1563-5287 online
DOI: 10.1080/15421406.2011.581119

Taylor & Francis
Taylor & Francis Group

Nematicon Self-Steering

ARMANDO PICCARDI, ALESSANDRO ALBERUCCI, AND GAETANO ASSANTO*

NooEL, Nonlinear Optics and OptoElectronics Lab, University "Roma Tre", Via della Vasca Navale 84, Rome-Italy

We report on nematicon self-steering in two settings: pure nematic liquid crystals, where the steering stems directly from optical reorientation, and dye-doped liquid crystals, where strong confinement owing to a guest-host interaction allows the appearance of a transverse force acting on the beam.

1. Introduction

Optical spatial solitons [1] are transversely self-localized waves stemming from the balance between linear diffraction and (effective) self-focusing in nonlinear materials [2–5]. In the past decades the investigation of fundamental processes ruling the formation of such optical structures brought about the comprehension of solitions stabilized in two-dimensions by nonlocality [6], their robustness to perturbations and their features as self-induced waveguides. All these properties make them excellent candidates for the next generation of electro- or opto-optical systems for signal routing and processing [7].

Among the most employed materials for solitons, nematic liquid crystals (NLC) are quite intriguing as they exhibit a large birefringence, hence remarkably high walk-off angles, and a high reorientational nonlinearity, stemming from dipolar interactions between the light electric field and the elongated molecules [8]. Moreover, NLC show a highly nonlocal response due to long-range elastic intermolecular forces [9]. Most NLC behave optically as positive uniaxials, with the optic axis corresponding to the mean molecular orientation, i.e. the *director* $\boldsymbol{n}$, and the dielectric tensor given by $\varepsilon_{jk} = \varepsilon_\perp \delta_{jk} + (\varepsilon_{||} - \varepsilon_\perp) n_j n_k$ *(j,k = x,y,z)*, with $\varepsilon_{||} = n_{||}^2$ and $\varepsilon_\perp = n_\perp^2$ the eigenvalues parallel and perpendicular to $\boldsymbol{n}$, respectively, and $n_j (j = x, y, z)$ the components of $\boldsymbol{n}$ in a Cartesian reference system.

In recent years, optical spatial solitons in NLC - or Nematicons [10] - have been studied in a number of geometries and nonlinear regimes [11–18], employing in- and out-of-plane interactions either between solitons [19,20] or with electrically and/or optically induced index perturbations [21–24]. Strategies have been proposed for nematicon-based optical signal processing and routing [19,25,26].

In this work we investigate nematicon self-steering, i.e. power-driven deflection of self-confined beams, both in pure and dye-doped NLC: in the former case beam self-deflection is possible via strong light-induced reorientation, in the latter it is due to the appearance of a transverse force stemming from non-paraxial effects. Soliton self-steering was previously observed in photorefractives owing to asymmetric diffusion of photo-induced charges, [27]

*Corresponding author. E-mail: assanto@uniroma3.it

and in parametric dielectrics by phase-locking between fundamental and second-harmonic waves in the presence of anisotropy [28,29].

2. Model

We refer to a planar cell of thickness L along x, infinitely extended along y and limited in z by input and output interfaces (Fig. 1(a)), with the director able to rotate in the plane yz: its distribution is fully described by the angle $\theta = \boldsymbol{n}\angle\hat{z}$, i.e. $\theta = \boldsymbol{n}\angle\boldsymbol{k}$ for beam launched with wave-vector $\boldsymbol{k}//\hat{z}$. At rest, i.e. for zero optical intensity, we assume $\theta = \theta_0$ everywhere, with θ_0 fixed by mechanical rubbing of the surfaces confining the NLC layer. In the highly nonlocal regime and under the Slowly Varying Envelope Approximation (SVEA), the propagation of an extraordinarily polarized beam with wave-vector along z is ruled by a nonlinear Schrödinger-like equation (NLSE) [30]:

$$2ik_0 n_e^{(b)}\left(\frac{\partial A}{\partial z} + \tan\delta^{(b)}\frac{\partial A}{\partial y}\right) + D_y\frac{\partial^2 A}{\partial y^2} + \frac{\partial^2 A}{\partial x^2} + k_0^2\Delta n_e^2 A = 0 \tag{1}$$

where $A = H_x e^{-ik_0 n_e^{(b)} z}$ is the envelope of the magnetic field (polarized along x), k_0 the vacuum wave-number, n_e the extraordinary refractive index, $\delta = \delta(\theta)$ the walk-off, D_y the diffraction coefficient along y and $\Delta n_e^2 = n_e^2(\theta) - \left(n_e^{(b)}\right)^2$ the nonlinear change in index due to reorientation. The superscript "*(b)*" indicates values (of walk-off and extraordinary index) computed on beam axis: in the highly nonlocal limit we can assume that walk-off does not change across the transverse profile of the beam. The corresponding extraordinary electric field is $E_t = -Z_0/(n_e^{(b)}\cos\delta^{(b)})H_x$ (with Z_0 the vacuum impedance) and forms an angle $\delta^{(b)}$ with y.

Setting $\theta = \theta_0 + \varphi$, with φ the optically induced reorientation, the reorientation equation in the single elastic constant approximation reads [9,30]:

$$\nabla^2\varphi + \gamma\,|E_t|^2\sin[2\left(\theta_0 + \varphi - \delta^{(b)}\right)] = 0 \tag{2}$$

with $\gamma = \varepsilon_0(n_{||}^2 - n_\perp^2)/4K$ and K the Frank elastic constant. Solving Eq. (2) we can find the parameters (walk-off, nonlinear index, diffraction coefficients) to be inserted in Eq. (1) and allowing to calculate the beam profile versus propagation and excitation; the profile,

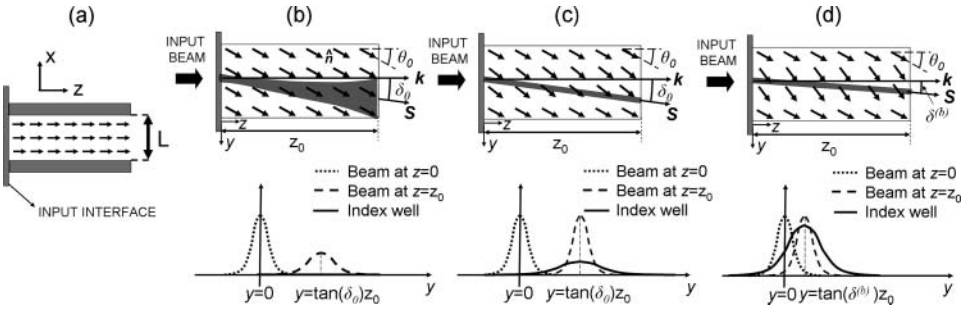

Figure 1. (a) Side view of the planar NLC cell. (b) Linear optical propagation in the plane yz (top view); (c) yz nonlinear optical propagation in the perturbative regime; (d) yz nonlinear optical propagation in the non-perturbative regime.

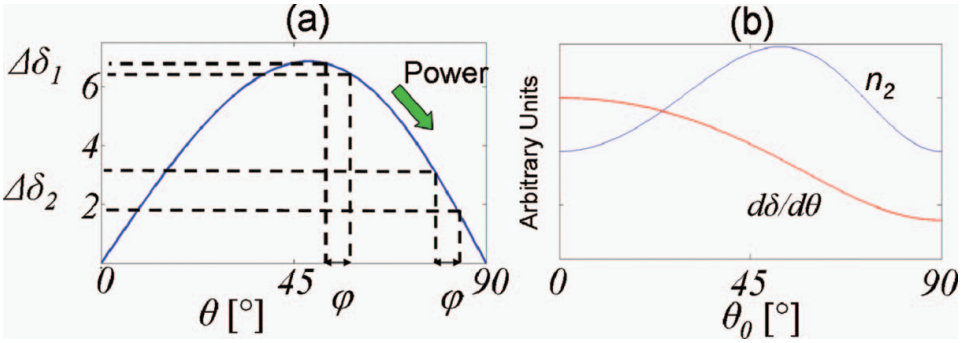

Figure 2. (a) Calculated walk-off versus angle θ between wave-vector and director, for $n_{//} = 1.7$ and $n_{\perp} = 1.5$. The arrow indicates variations due to increasing optical excitation. (b) Calculated nonlocal Kerr coefficient n_2 and derivative of walk-off δ_0 versus θ_0.

in turn, governs the transverse director distribution via Eq. (2). Thus Eqs. (1–2) form a self-consistent system by which light self-effects in NLC can be studied when reorientation is the dominant nonlinear effect.

By increasing the input power, three different regimes can be expected for optical beam propagation. At low powers, i.e. in the linear regime (Fig. 1(a)), the all-optical reorientation φ is negligible and light linearly diffracts, with the Poynting vector forming an angle $\delta_0 = \delta(\theta_0)$ with respect to z. At higher power φ is no longer negligible and can induce self-trapping via the term $k_0^2 \Delta n_e^2 A$ in Eq. (1). A perturbative (Fig. 1(c)) and a non-perturbative regime (Fig. 1(d)) can be identified. In the perturbative regime the optical reorientation φ is negligible with respect to the initial angle θ_0; in the non-perturbative regime φ becomes comparable to θ_0. In the former case, similar to the linear one, the walk-off is determined by the initial director distribution, whereas in the latter it depends on beam power.

In the perturbative regime it is straightforward to find a nonlocal effective Kerr coefficient by using the Green function formalism [30]:

$$n_2(\theta_0) = 2\gamma \sin\left[2\left(\theta_0 - \delta_0\right)\right] n_e^2(\theta_0) \tan\delta_0 \tag{3}$$

Equation (3) relates the nonlinearity to the material parameters via γ and to the sample geometry through θ_0. By maximizing Eq. (3) versus θ_0, it appears that $\theta_0 \approx \pi/4$ is the best value for soliton self-steering (Fig. 2(b)), since small variations in power lead to large reorientation; however, as apparent from Fig. 2, around $\theta_0 = \pi/4$ the walk-off derivative is nearly zero, thus preventing any detectable beam deflection even in the presence of strong reorientation; conversely, its sensitivity increases towards $\theta_0 = 0$ or $\theta_0 = \pi/2$: a trade-off is therefore necessary between $n_2(\theta_0)$ and $\delta(\theta_0)$.

3. Self-Steering in Undoped Nematic Liquid Crystals

To solve our problem numerically, firstly we reduce it to a 2D geometry, retaining only the first term in the Fourier expansion of the optical perturbation, i. e. $\varphi(x, y, z) = \sin(\pi x/L)\,\Phi(y, z)$, and setting boundary conditions at the confining interfaces $x = 0, L$ (Fig. 1(a)). Eq. (2) becomes a Yukawa-like equation [30]:

$$\nabla_{yz}^2 \Phi - \left(\frac{\pi}{L}\right)^2 \Phi + \gamma \sin\left[2\left(\theta_0 + \Phi - \delta\right)\right] |E_t|^2 = 0 \tag{4}$$

accounting for the actual nonlocality of the 3D case through the screening term. We further write Eq. (1) in the limit $A(x, y, z) = \Theta(x, z)\Psi(y, z)$ and integrate it along x, obtaining the 2D model:

$$2ik_0 n_e^{(b)} \left(\frac{\partial \Psi}{\partial z} + \tan \delta^{(b)} \frac{\partial \Psi}{\partial y} \right) + D_y \frac{\partial^2 \Psi}{\partial y^2} + k_0^2 \Delta n_e^2 \Psi = 0 \tag{5}$$

where the nonlinear index well is computed in the cell mid-plane $x = L/2$. This approach reduces the computational effort but maintains the main physical features of the problem. To account for losses (mainly due to scattering) we consider power reduction in propagation $P = P_0 e^{-2\alpha z}$ (P_0 is the input power), with coefficient α estimated from experiments.

Using the system of Eqs. (4–5) we can analyze the power dependence of the beam trajectory for various initial angles θ_0. Figure 3 shows some results for $\alpha = 5\,\mathrm{cm}^{-1}$.

As anticipated in section 2, the maximum steering angle is found around $\theta_0 = 20, 70^\circ$. Noteworthy, the trajectories are curved rather than straight: this is due to losses, which gradually reduce reorientation versus z until, for $z \gg \alpha^{-1}$, the system goes back to the linear limit.

We performed experiments in a sample of E7 with thickness $L = 100\ \mu$m. A Nd-YAG laser beam at $\lambda = 1064$ nm was focused into the cell and excited an extraordinarily polarized wave. The beam evolution was monitored by a CCD camera collecting the scattered light. To vary θ_0 we used a cell with two Indium-Tin-Oxide comb-like electrodes to electrically control the in-plane reorientation: each applied voltage corresponded to a value of initial angle θ_0. The main results are shown in Fig. 4 and reproduce the predictions: maximum self-deflection was observed for $\theta_0 = 20^\circ$ and $\theta_0 = 70^\circ$, while for $\theta_0 \approx 45^\circ$ no power dependence could be detected in phe power range $P \in [1\text{–}10]\,mW$.

Figure 5 shows the comparison between numerical and experimental soliton deviation from the perturbative regime: due to saturation, a slightly asymmetric behaviour is observed at angles close to 90°.

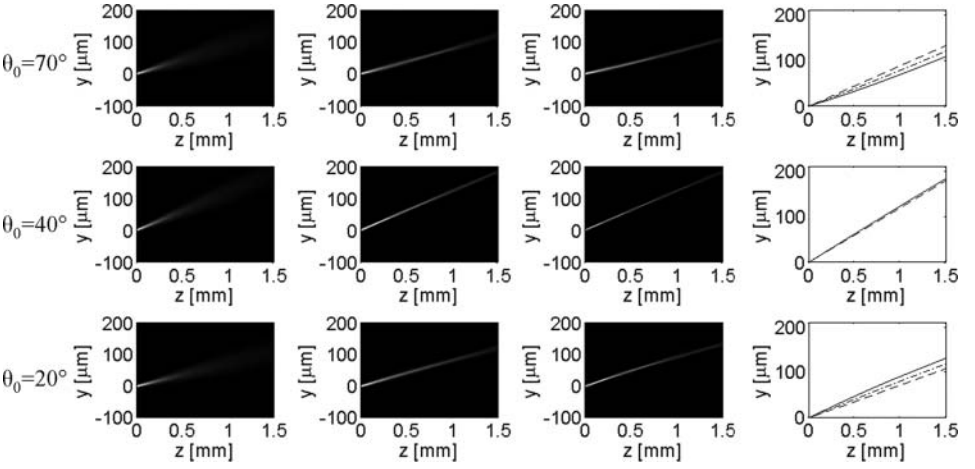

Figure 3. BPM simulations of soliton self-steering in undoped NLC. Each row corresponds to a specific θ_0. The first three columns display the beam evolution in yz for $P_0 = 1\ \mu$W, 1 and 2 mW, respectively, whereas the last column plots the corresponding beam trajectories, with dashed, dashed-dotted and solid lines corresponding to increasing powers.

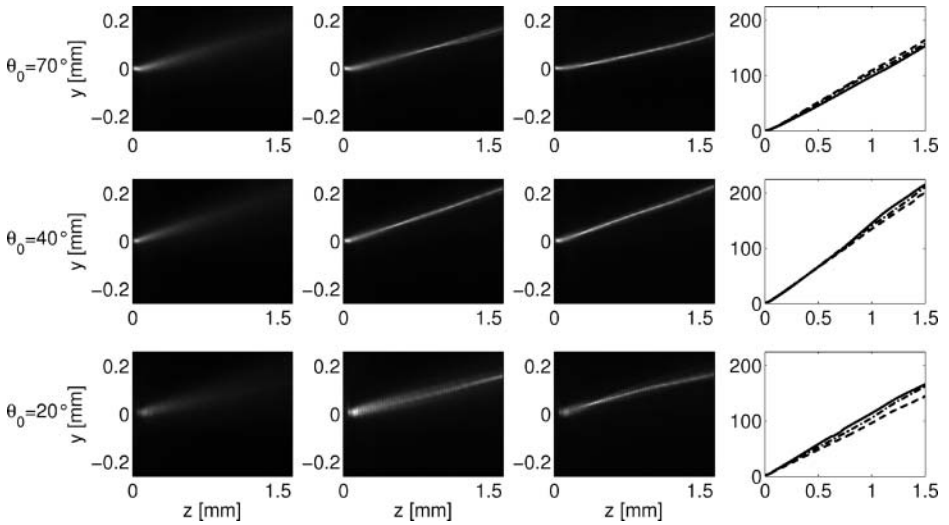

Figure 4. Soliton self-steering in undoped NLC. Each row corresponds to an initial θ_0. The first three columns show photos of beam evolution for various powers, namely $P_0 = 1, 5, 10$ mW, respectively. The last column plots the measured trajectories. Dashed, dashed-dotted and solid lines correspond to $P_0 = 1, 5, 10$ mW, respectively.

4. Self-Steering in Dye-Doped Nematic Liquid Crystals

In the previous sections we predicted and experimentally verified that nematicon self-deflection takes place when optical reorientation is comparable to the initial orientation angle. In this section we focus on a specific dye-doped nematic liquid crystals (DDNLC).

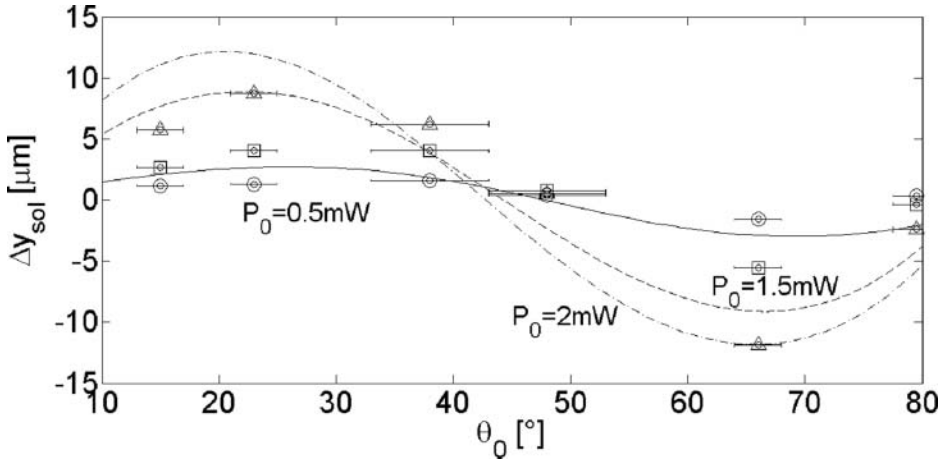

Figure 5. Nematicon displacement computed at $z = 500\,\mu$m with respect to the linear trajectory $y_{sol} = \tan(\delta_0)z$ versus rest angle θ_0. Circles, squares and triangles are experimental data for $P_0 = 2{,}5{,}10$ mW, respectively. Solid, dashed and dashed-dotted lines are numerical simulations (Eqs. (4–5)) for initial power as indicated. The error bars derive from uncertainties in walk-off measurements.

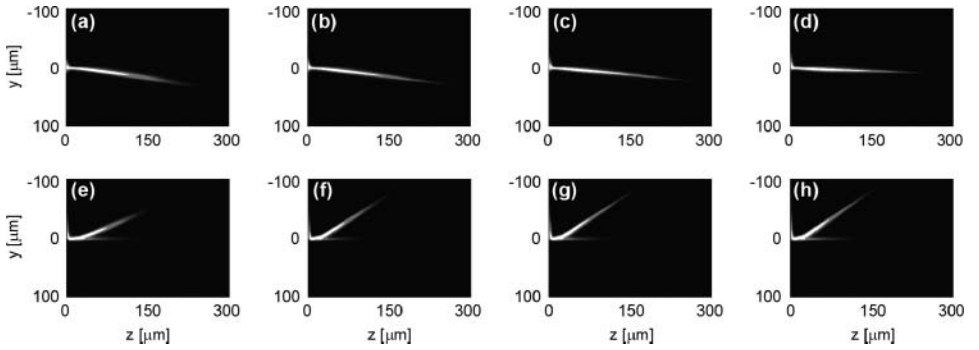

Figure 6. Nematicon self-steering in DDNLC. Photos of emitted red light trapped in the blue induced soliton waveguide. (a) For $P_0 = 80$ μW the beam diffracts and the Poynting vector walks off at about 9°. For $P_0 = 120$ (b), *180* (c), 220 μW (d), respectively, self-confinement takes place and the soliton self-steers until its trajectory is parallel to z. Due to non-paraxial effects, for $P_0 = 240$ (e), 300 (f), 340 (g), 400 μW (h), respectively, the beam further steers up to $-30°$.

In DDNLC the so-called *Janossy effect*, due to dye-mediated enhancement of the interaction between optical field and induced molecular dipoles [31], is known to enhance all-optical reorientation; hence, we expect larger beam steering in the same power range. Using the sample geometry of Fig. 1, we used a mixture of E7 and 1-Amino-Anthraquinone (1-AAQ) [32], in a ratio 100:1 in weight. To optimize the trade-off between detectable effects and tolerable absorption, we employed a He-Cd laser of wavelength $\lambda = 442$ nm, i.e., within the absorption spectrum of 1-AAQ. As visible in Fig. 6, self-focusing occurred at sub-mW powers and, due to dye photoluminescence, collinear and co-polarized red photons were emitted and trapped in the blue nematicon-waveguide. As power was raised, the walk-off reduced from 9° (linear walk-off at the employed wavelength) to zero for $P_0 = 220$ μW; when power was further increased to $P_0 = 400$ μW the beam steered itself towards negative y (Fig. 6(e–h)) up to $-30°$.

Despite the large beam self-steering to be expected on the basis of an enhanced nonlinearity, the behavior is qualitatively different from what discussed in section 2. First, even in the presence of strong absorption (we measured $\alpha = 50$ cm^{-1}), the trajectories are straight; second, at high powers the Poynting vector walks off at a negative angle while an ordinary component appears (in the blue, not shown). This is not compatible with self-steering solely due to nonlinear changes in walk-off; it suggests the presence of an asymmetric potential tilting the wave-vector. Asymmetric profiles in refractive index due to either strong reorientation or heating, or stemming from the interaction between bent trajectories and boundary conditions at the input interface $z = 0$ were found to be negligible. The source of the asymmetry can be ascribed to the longitudinal field component $E_s = -j \cos\delta^{(b)}/(\omega\varepsilon_{zz})\, H_x$ (Fig. 7(a)). We therefore modify Eq. (2) into:

$$\nabla^2\varphi + \gamma(1+\eta)\{(|E_t|^2 - |E_s|^2)\sin[2(\theta_0 + \varphi - \delta^{(b)})] + 2\Re(E_t E_s^*) \times \cos[2(\theta_0 + \varphi - \delta^{(b)})]\} = 0 \tag{6}$$

with η the Janossy amplification [31] and subscripts "t" and "s" referring to transverse and longitudinal fields components, respectively.

Due to enhanced self-confinement, the paraxial approximation is no longer valid and the longitudinal field component becomes comparable with the transverse one (Fig. 7(b))

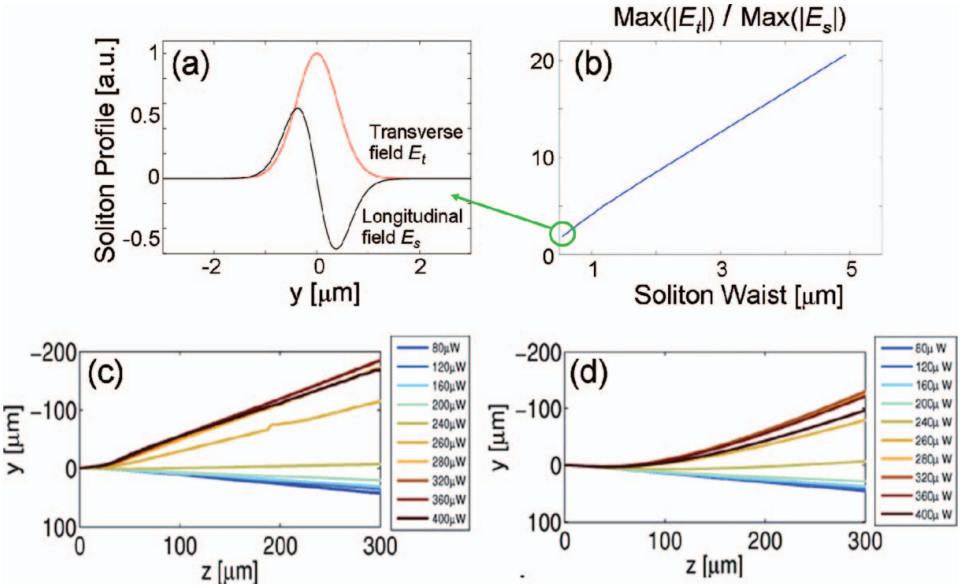

Figure 7. (a) Calculated transverse and longitudinal electric field components for a soliton waist of 0.5 μm. (b) Ratio between peaks of $|E_t|$ and $|E_s|$ versus waist. (c) Measured trajectories corresponding to Fig. 6 and (d) theoretical trajectories calculated with Eqs. (8).

and shows an odd symmetry (Fig. 7(a)). If the guest-host system lacks inversion symmetry, an odd refractive index potential can induce an effective transverse force on the solitary beam. For the latter, defining a phenomenological constant c_0 and naming β the nematicon propagation constant, in the highly nonlocal limit we can derive the expression [33]:

$$F = c_o \zeta e^{-\alpha z} P_0^{3/2} w^{-2} \tag{7}$$

with ζ a constant depending on material, sample geometry and maximum reorientation, and w the soliton waist. Hence, the soliton evolution can be calculated through [33]

$$\begin{aligned} \frac{d^2 y_b}{dz^2} &= \frac{d \tan \delta^{(b)}}{dz} + F \\ \frac{d^2 w}{dz^2} &= -\left(\sigma \frac{\sqrt{P}}{w}\right)^2 (w - w_0) \end{aligned} \tag{8}$$

the first equation describing the evolution of the solition centre of mass y_b as dictated by the Ehrenfest's theorem and the second ruling the waist evolution in highly nonlocal media, with w_0 the soliton waist for a given power.

By fitting the constant c_0 to the experimental data, we obtained a good agreement between measured and calculated trajectories (Fig. 7(c–d)), with a maximum self-steering of 39 degrees (Fig. 8). The Fréedericksz-like transition in c_0 (Fig. 8 right) suggests that dye-mediated reorientation occurs out of the plane yz, thereby explaining the appearance of ordinary waves at large powers. Since a coupling of ordinary and extraordinary components requires a non-asymptotic variation in director distribution, considering that nonlocality prevents DDNLC properties in bulk from changing on scales much shorter than L, soliton

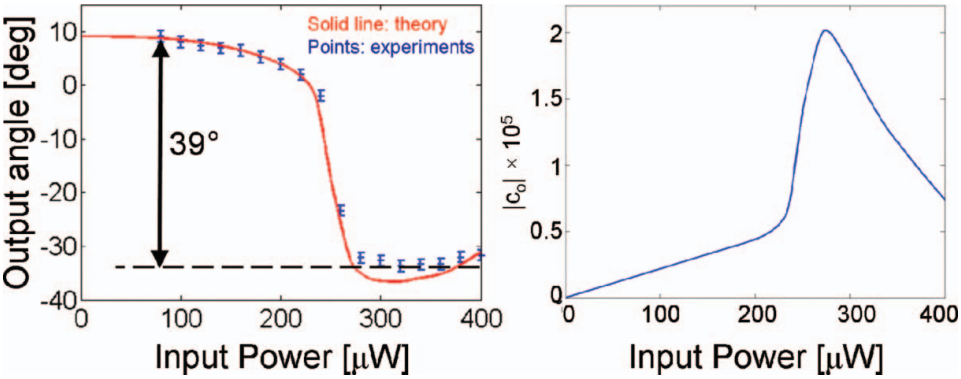

Figure 8. Left: measured (points) and theoretical (solid line) angle between the Poynting vector and axis z, taken at the output section and versus input power. Right: fit-coefficient c_0 found by fitting experimental data with predictions from Eqs. (8). A saturating behavior for $P_0 > 250\ \mu$W is consistent with saturation in reorientation.

self-steering and ordinary wave generation occurred in proximity of the input interface, where the molecular distribution can change on lengths shorter than L (Fig. 7(c)).

5. Conclusions

In conclusion, we discussed and reported power-controlled soliton self-deflection in liquid crystals. Steering in an undoped material is due to nonlinear changes in walk-off via the large light-induced reorientation, this effect rather dependent on initial director orientation. In a guest-host system such as dye-doped nematic liquid crystals E7 with 1-AAQ, non-paraxial propagation due to the Janossy effect can yield an odd refractive potential and introduce an effective transverse force able to deviate the beam wave-vector; this angular steering effect persists even at those large propagation distances where the beam should have retrieved its linear properties owing to losses.

Acknowledgments

We are grateful to M. Peccianti, M. Kaczmarek and S. Residori. Effort partially sponsored by the Air Force Office of Scientific Research, Air Force Material Command, USAF, under grant number FA-8655-10-1-3010. The U.S. Government is authorized to reproduce and distribute reprints for Governmental purpose notwithstanding any copyright notation thereon.

References

[1] Stegeman, G. I., & Segev, M. (1999). *Science*, *286*, 1518–1523.
[2] Bjorkholm, J. E., & Ashkin, A. A. (1974). *Phys. Rev. Lett.*, *32*, 129–132.
[3] Duree, G. C., Shultz, J. L., Salamo, G. J., Segev, M., Yariv, A., Crosignani, B., Di Porto, P., Sharp, E.J., & Neurgaonkar, R.R. (1993). *Phys. Rev. Lett.*, *71*, 533–536.
[4] Canva, M. T. G., Fuerst, R. A., Baboiu, S., Stegeman, G. I., & Assanto, G. (1997) *Opt. Lett.*, *22*, 1683–1685; Assanto, G., & Stegeman, G. I. (2002). *Opt. Express*, *10*, 388–396.
[5] Rotschild, C., Cohen, O., Manela, O., Segev, M., & Carmon, T. (2005). *Phys. Rev. Lett.*, *95*, 213904.

[6] Suter, D., & Blasberg, T. (1993) *Phys. Rev. A*, *48*, 4583–4587.
[7] Conti, C., & Assanto, G. (2004) "Nonlinear Optics Applications: Bright Spatial Solitons", *Encyclopedia of Modern Optics*, *5*, 43–55, edited by R. D. Guenther, D. G. Steel and L. Bayvel, Elsevier: Oxford.
[8] Conti, C., Peccianti, M., & Assanto, G. (2003). *Phys. Rev. Lett.*, *91*, 073901.
[9] Simoni, F. (1997). *Nonlinear Optical Properties of Liquid Crystals*, World Scientific: Singapore.
[10] Assanto, G., Peccianti, M., & Conti, C. (2003). *Opt. Photon. News*, *14*, 44–48.
[11] Braun, E., Faucheux, L. P., & Libchaber, A. (1993). *Phys. Rev. A*, *48*, 611.
[12] Karpierz, M.A. (2002). *Phys. Rev. E*, *66*, 036603.
[13] Peccianti, M., Assanto, G., De Luca, A., Umeton, C., & Khoo, I. C. (2000). *Appl. Phys. Lett.*, *77*, 7–9.
[14] Peccianti, M., Conti, C., Assanto, G., De Luca, A., & Umeton, C. (2004). *Nature*, *432*, 733–737.
[15] Derrien, F., Henninot, J.F., Warenghem, M., & Abbate, G. (2000). *J. Opt. A: Pure Appl. Opt.*, *2*, 332–338.
[16] Peccianti, M., & Assanto, G. (2002). *Phys. Rev. E*, *65*, 035603.
[17] Piccardi, A., Bortolozzo, U., Residori, S., & Assanto, G. (2009). *Opt. Lett.*, *34*, 737.
[18] Piccardi, A., Peccianti, M., Assanto, G., Dyadyusha, A., & Kaczmarek, M. (2009). *Appl. Phys. Lett.*, *94*, 091106.
[19] Peccianti, M., Conti, C., Assanto, G., De Luca, A., & Umeton, C. (2002). *Appl. Phys. Lett. 81*, 3335–3337.
[20] Fratalocchi, A., Piccardi, A., Peccianti, M., & Assanto, G. (2007). *Opt. Lett.*, *32* (11), 1447–1449.
[21] Pasquazi, A., Alberucci, A., Peccianti, M. & Assanto, G. (2005). *Appl. Phys. Lett.*, *87*, 261104.
[22] Serak, S. V., Tabiryan, N.V., Peccianti, M., & Assanto, G. (2006). *IEEE Photon. Techn. Lett.*, *18*, 1287–1289.
[23] Peccianti, M., Assanto, G., Dyadyusha, S., & Kaczmarek, M. (2006). *Nature Phys.*, *2*, 737–742.
[24] Piccardi, A., Assanto, G., Lucchetti, L., & Simoni, F. (2008). *Appl. Phys. Lett.*, *93*, 171104.
[25] Assanto, G., & Peccianti, M. (2008). *Mol. Cryst. Liq. Cryst.*, *488*, 163.
[26] Piccardi, A., Alberucci, A., Bortolozzo, U., Residori, S., & Assanto, G. (2010). *IEEE Photon. Techn. Lett.*, *22*, 694–696.
[27] Shih, M., Leach, P., Segev, M., Garrett, M.H., Salamo, G., & Valley, G.C. (1996). *Opt. Lett.*, *21*, 324–326.
[28] Torruellas, W. E., Assanto, G., Lawrence, B. L., Fuerst, R. A., & Stegeman, G. I. (1996). *Appl. Phys. Lett.*, *68*, 1449–1451.
[29] Gallo, K., Pasquazi, A., Stivala, S., & Assanto, G. (2008). *Phys. Rev. Lett.*, *100*, 053901
[30] Alberucci, A., Piccardi, A., Peccianti, M., Kaczmarek, M., & Assanto, G. (2010). *Phys. Rev. A*, *82*, 023806.
[31] Janossy, I., Lloyd, A., & Wherrett, B. (1990). *Mol. Cryst. Liq. Cryst.*, *179*, 1 (1990).
[32] Inoue, H., Hoshi, T., Yoshino, J., & Tanizaki, Y. (1972). *Bull. Chem. Soc. Jpn.*, *45*, 1018.
[33] Piccardi, A., Alberucci, A., & Assanto, G. (2010). *Phys. Rev. Lett.*, *104*, 213904.